第49卷第12期 中国科学技术大学学报 Vol. 49, No. 12
2019年12月 JOURNAL OF UNIVERSITY OF SCIENCE AND TECHNOLOGY OF CHINA Dec. 2019

文章编号:0253-2778(2019)12-0995-07

Carbon nanofibers by electrospun for high-performance supercapacitors

PAN Shiquan, JIN Hongchang, QI Zhikai, JI Hengxing

(*Hefei National Laboratory for Physical Sciences at the Microscale, CAS Key Laboratory of Materials for Energy Conversion, Department of Applied Chemistry, University of Science and Technology of China, Hefei* 230026, *China*)

Abstract: Recently, metal-organic frameworks (MOFs) have been regarded as an ideal precursor for preparing nanoporous carbon materials for the electrodes of supercapacitors due to their ability to tune the material's structure from the molecular scale. However, the MOF-derived carbons usually exhibit a low graphitization level and large interface resistance between the particles which yield a poor electrical conductivity of the electrode disc that greatly limits their electrochemical performance. Herein, we demonstrate that pyrolysis of ZIF-67 that is embedded into a nanowire network made of polyacrylonitrile (PAN) can achieve a freestanding carbon-based electrode for supercapacitors. PAN nanowires yield pyrolytic carbon of high graphitization level to connect ZIF-derived carbon nanoparticles for efficient charge transfer; ZIF-67 provides nitrogen doped porous carbon structure for charge storage. Such a electrode delivered a gravimetric capacitance of 124 $F \cdot g^{-1}$ at the current density of 1 $A \cdot g^{-1}$ with a capacitance retention of greater than 92% over 10 000 cycles at 10 $A \cdot g^{-1}$.

Key words: electrospun; carbonized nanofiber; supercapacitor

CLC number: TM53 **Document code**: A doi:10.3969/j.issn.0253-2778.2019.12.006

Citation: PAN Shiquan, JIN Hongchang, QI Zhikai, et al. Carbon nanofibers by electrospun for high-performance supercapacitors[J]. Journal of University of Science and Technology of China, 2019, 49(12): 995-1001.

潘士泉,金洪昌,齐志凯,等. 用于高性能超级电容器的电纺碳纤维材料[J]. 中国科学技术大学学报, 2019, 49(12): 995-1001.

用于高性能超级电容器的电纺碳纤维材料

潘士泉, 金洪昌, 齐志凯, 季恒星

(中国科学技术大学合肥微尺度物质科学国家研究中心, 中国科学院能源转换材料重点实验室, 中国科学技术大学应用化学系, 安徽合肥 230026)

摘要: 金属有机骨架(MOFs)被认为是制备纳米多孔碳材料并用于超级电容器电极的理想前体,因为它们能够从分子尺度调节材料的结构.但是,一方面 MOFs 衍生的碳通常表现出较低的石墨化水平,另一方面纳米多孔碳颗粒之间具有较大的界面电阻,这些影响因素会导致电极的导电性差,进而极大地限制它们的电化学性能.本研究成功将 ZIF-67 嵌入聚丙烯腈(PAN)的纳米线纤维中,并在碳化处理后可以独立地用于超级电容器电极.PAN 纳米纤维在热解过程中能够产生高石墨化水平的碳纤维,一方面用于连接 ZIF 衍生的碳

Received: 2019-04-28; **Revised**: 2019-06-14

Foundation item: Supported by National Natural Science Foundation of China (51761145046).

Biography: PAN Shiquan, male, born in 1994, master candidate. Research field: carbon materials. E-mail: panshiq@mail.ustc.edu.cn

Corresponding author: JI Hengxing, PhD/Prof. E-mail: jihengx@ustc.edu.cn

纳米颗粒,另一方面有利于电荷转移;ZIF-67 可以提供氮掺杂的多孔碳结构用于电荷存储.这种电极在 1A·g^{-1} 的电流密度下可以达到 124F·g^{-1} 的质量比容量,并在 10A·g^{-1} 的 10 000 次循环中电容保持率大于 92%.

关键词:静电纺丝;碳纳米纤维;超级电容器

0 Introduction

Supercapacitors, also called ultracapacitors or electrochemical capacitors, have attracted great attention owing to their high power density and long cycle life[1-4], which store energy by forming an electric double-layer at the interface between liquid electrolyte and the electrode[5]. The physical properties of the electrode materials, for instance the porous structure, surface area, electrical conductivity, and chemical stability, etc., dominate the electrochemical performance of the supercapacitors[1,6]. The widely used electrode materials mainly include carbon materials, metal oxides, and conducing polymer, in which nanoporous carbons (NPCs) are considered to be the most promising ones because of their relatively high electrical conductivity, excellent chemical stability, controllable porous structure, and rich carbon sources[7-11].

In recent years, metal-organic framework (MOF) has drawn much attention for obtaining NPCs owing to its high specific surface area (SSA) and its richness in heteroatoms that can yield highly doped NPCs. These features are critical for NPCs to yield improved gravimetric capacitance. Direct carbonization of MOF by thermal treatment in an inert atmosphere is the most wildly used method[12-15]. In 2008, for the first time, Liu et al.[19] reported an NPC obtained by direct carbonization of MOF-5, which showed a specific surface area of 2 872 $m^2 \cdot g^{-1}$ and promising gravimetric capacitance of 258 F·g^{-1} at 250 mA·g^{-1}. Recently, Deng et al.[20] used $Co(OH)_2$ as both the template and precursor to fabricate a vertically-oriented MOF electrode for high-performance supercapacitors. Despite the feasibility in structure tuning, the inherent limitations of MOF-derived NPCs still hinder its applications for supercapacitors, for example the poor graphitization level of the carbonized MOFs and the interface resistance between the NPCs particles that lower the electrical conductivity, and thus lead to a restricted power density[21-22].

In this work, we fabricated a binder-free N-doped carbonized nanofibers (CNFs-N) using ZIF-67 embedded polyacrylonitrile (PAN) as precursor through electrospinning. The carbonized ZIF-67 nanoparticles are interconnected by carbonized PAN fibers which facilitates electron transfer during the charge-discharge process. In addition, ZIf-67 and PAN also provide a nitrogen source to generate N-dopants in carbon , which enhances the overall capacitacity. Thus, our CNFs-N delivered a gravimetric capacitance of 124 F·g^{-1} at the current density of 1 A·g^{-1} with a high capacitance retention of greater than 92% over 10 000 cycles.

1 Experimental

1.1 Preparation of ZIF-67 particles

Typically, 3.446 g of $Co(NO_3)_2 \cdot 6H_2O$ was dissolved in 120 mL of methanol. 7.787 g of 2-methylimidazole (MeIM) was dissolved in 120 mL of methanol. Then, the two solutions were rapidly mixed together under magnetic stirring at room temperature. After stirring for 1 h at room temperature, the purple powder was collected by centrifugation at 9 000 r/min for 10 min, and was washed three times with methanol.

1.2 Preparation of N-doped carbon nanofibers (CNFs-N)

0.39 g of the as-synthesized ZIF-67 powder was dispersed in 2 mL of dimethylformamide (DMF) solvent with the assistance of ultrasound for 2 h. Then 0.26 g of polyacrylonitrile (PAN, average MW 150 000) was dispersed in the ZIF-67/DMF suspension. The mixture was stirred for 24 h to form a homogeneously suspension. Then, the

mixture was loaded into a syringe (5 mL) with a stainless-steel nozzle which was connected to a high-voltage power supply. The voltage, feeding rate, temperature, and distance between the anode and cathode are fixed at 20 kV, 3.5 mm·h^{-1}, 25 ℃, and 15cm, respectively. The electrospun ZIF-67/PAN film was dried at 45 ℃ for 12 h in vacuum. Carbonization was carried out through a two-stage heating process. Specifically, the sample was held to 270 ℃ with a ramping rate of 5 ℃·min^{-1} in air and the temperature was held at 270℃ for 1 h. Then the sample was heated to 800 ℃ with a ramping rate of 5 ℃·min^{-1} under the protection of N_2 gas. The temperature was held at 800℃ for 2 h before cooling down to room temperature. Subsequently, the resultant materials were washed thoroughly in a H_2SO_4 solution (2.0 mol·L^{-1}). Finally, the as-obtained CNFs-N sample was rinsed with deionized water and dried in vacuum at 45 ℃. The carbonized ZIF-67 and electronspun PAN film were obtained by carbonization through the same heating process for CNFs-N.

1.3 Material characterization

The morphology of the samples was examined using a scanning electron microscope (SEM, JSM-6700F) and a field-emission transmission electron microscope (FETEM, JEM-2100F). The crystal phase of the products was examined by X-ray diffraction spectroscopy (XRD, D/max-TTR III) with Cu Kα radiation (V=40kV, I=200mA) with scan rate of 5°·min^{-1} from 10° to 50° (2θ). Raman scattering spectra were collected on a Raman spectroscopy (Renishaw inVia Raman Micro-scope, 532 nm laser with a power of 5 mW). X-ray photoelectron spectroscopy (XPS) spectra were obtained on an ESCA Lab MKII X-ray photoelectron spectrometer with a Mg Kα (1 253.6 eV) excitation source. The surface area and pore size distribution of samples were calculated with N_2 adsorption-desorption using a Quanta chrome instrument (autos orb iQ2) with Brunauer-Emmett-Teller (BET) methods and quenched solid density functional theory (QSDFT) model.

1.4 Electrochemical measurements

All electrochemical measurements were carried out using a two-electrode system with a Versa Studio electrochemical workstation at room temperature. Before the assembly of the supercapacitors, the electrodes were soaked in aqueous H_2SO_4 electrolyte (2.0 mol·L^{-1}) for 48 h. The employed two-electrode configuration consisted of two slices of electrode materials with the same size (ø = 1.0 cm), PTFE filter paper (pore size: 225 nm) as the separator, and a pair of Pt plate as the current collectors. The areal density of the supercapacitor electrode was estimated by direct mass and physical dimension measurements, which is about 1.2 mg·cm^{-2}. CV and galvanostatic charge-discharge measurements were recorded at the working voltage of 0.0 to 1.0 V. The electrode was prepared by a directly carbonized sample without any binders.

The mass based specific capacitance (C_s) was calculated from the galvanostatic discharge process using the equation:

$$C_s = \frac{2I_{\text{cons}}}{m\,\mathrm{d}V/\mathrm{d}t}$$

where I_{cons} (A) corresponds to the constant discharge current, $\mathrm{d}V/\mathrm{d}t$ (V·s^{-1}) represents the slope of the discharge curve, and m (g) refers to the mass of the active material on the two electrodes.

2 Results and disscusion

Fig. 1(a) shows the processes for synthesizing the CNFs-N. Firstly, the ZIF-67 powder (synthesized according to Ref. [23]) was dispersed in dimethylformamide (DMF) solvent via sonication for 2 h followed by the addition of PAN powder. The mixture of a ZIF-67 : PAN : DMF at mass ratio of 1.5 : 1 : 7.5 was then stirred for 24 h to form a homogeneous dispersion. Then, the obtained suspension was subjected to electrospun to form the ZIF-67/PAN film on aluminum foil (Fig. 1(b)). The film with an area of 13.0cm × 18.0cm can be obtained within 300

min. The scanning electron microscopy (SEM) image (Fig. 1(c)) shows that the ZIF-67/PAN film obtained by electronspun is composed of fibers with a diameter of less than 1 μm and a length of tens of micrometers. After carbonization at 800 ℃ in N_2, the film is black yet still integrative, and the fibrous structure is preserved (Fig. 1(d)).

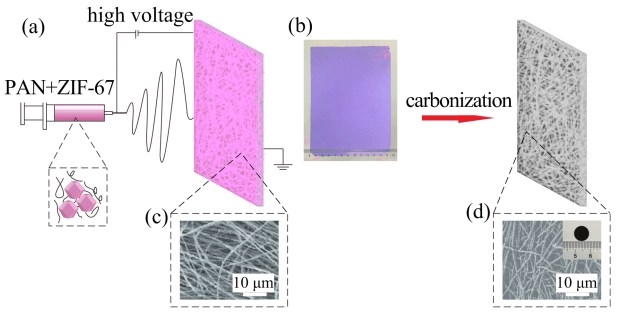

Fig. 1 (a) Schematic of the synthesis processes for CNFs-N, (b) optical photograph of ZIF-67/PAN fibers, (c) SEM image of ZIF-67/PAN fibers, (d) SEM image of CNFs-N. Inset in (d): photograph of CNFs-N

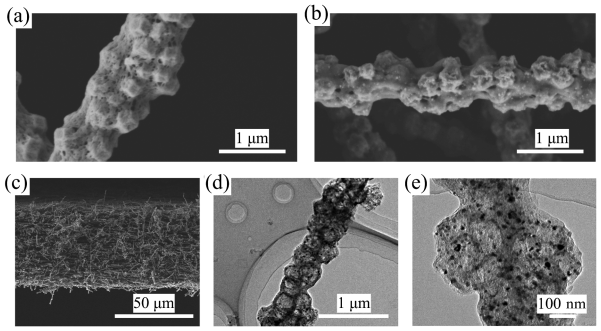

Fig. 2 SEM images of (a) ZIF-67/PAN and (b) CNFs-N fibers, (c) SEM image showing the cross section of a CNFs-N film, (d) and (e) TEM images of CNFs-N at different magnifications

The details of the microscale structure are further studied by SEM. Fig. 1(a) shows that the as-prepared ZIF-67/PAN composite nanofibers are very long and uniform in diameter (~1 μm) with nanoparticles of a diameter of around 200 nm embedded in the fibers. These nanoparticles which are not observed on the electrospun PAN fibers should be the ZIF-67 particles. After carbonization and acid washing, the resultant CNFs-N sample retains the fiber-like microscopy like that of the ZIF-67/PAN except that the structure of ZIF-67 particles and PAN fibers are slightly shrunk (Fig. 2(b)). Therefore, the diameter of the CNFs-N fibers is slightly reduced to around 700 nm. Benefitting from the network formed by the electrospun ZIF-67/PAN nanofibers, the obtained CNFs-N sample exhibits good self-standing ability (inset of Fig. 1(d)). The cross section of SEM image (Fig. 2(c)) shows uniform thickness of CNFs-N, and also the thickness is controllable by adjusting the spinning time (Fig. 2(c)). The TEM images (Fig. 2(d)) further reveal the microstructure of the CNFs-N. The nanofiber is composed of hollow nanoparticles interconnected with each other, which should be the carbonized ZIF-67 particles. In addition, nanoparticles with a diameter of around 10nm is observed in Fig. 2(e) which can be assigned to Co nanoparticles, as confirmed by the selected area electron diffraction pattern.

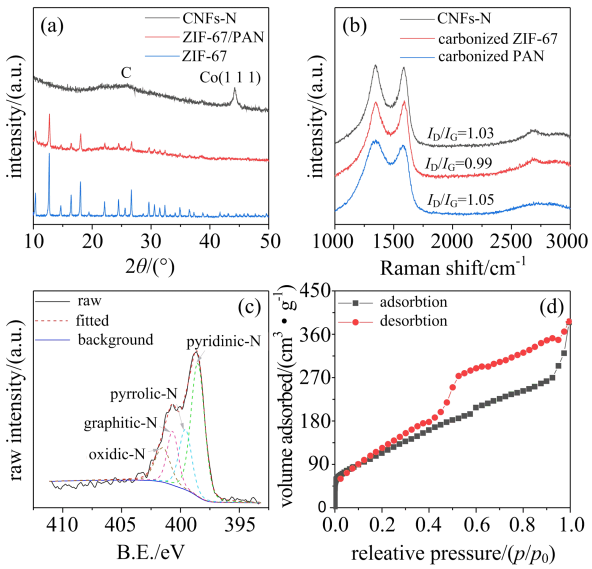

Fig. 3 (a) XRD patterns and (b) Raman spectra of CNFs-N and the control samples, (c) N 1s XPS spectra of CNFs-N, (d) N_2 adsorption/desorption isotherms of the CNFs-N

X-ray diffraction (XRD) patterns of CNFs-N, ZIF-67/PAN, and ZIF-67 are shown in Fig. 3(a). The XRD pattern of ZIF-67/PAN (red curve in Fig. 3(a)) shows sharp yet weak diffraction peaks. The relative intensities and peak positions well match those of ZIF-67 (blue curve in Fig. 3(b)), which again confirms the successful incorporating of ZIF-67 in the PAN microfiber network. After

carbonization, the CNFs-N shows a strong XRD peak at around 44.2°, which can be ascribed to the lattice plane of (111) of metallic cobalt[11]. A broad XRD peak at 2θ of 26° is also observed which can be assigned to carbon of weak graphitization level[10]. Such weak graphitization level of the CNF-N is further confirmed by Raman spectrum (Fig. 3(b)), which shows broad D (at 1 338 cm^{-1}) and G (at 1 585 cm^{-1}) bands with D/G intensity ratio of 1.03. The D/G intensity ratio of the CNF-N is slightly higher than that of the carbonized PAN, yet is lower than that of the carbonized ZIF-67, which could be due to the existence of Co nanoparticles that can assist the graphitization of carbon at the elevated temperature of 800 ℃[24].

N atoms substitutionally doped in carbon are found to be able to improve the Fermi level of carbon so as to improve the gravimetric capacitance[25]. Here, ZIF-67 and PAN have the N atomic percents of 13.8% and 25.3%, respectively, therefore, direct carbonization of ZIF-67/PAN yields CNFs-N of N atomic percent of 6.3%. X-ray photoelectron spectroscopy (XPS) was used to further analyze the configuration of N dopants in the CNFs-N. The N 1s spectrum of CNF-N (Fig. 3(c)) can be fit with four peaks which are assigned to pyridinic-N (398.5 eV), pyrrolic-N (400.1 eV), graphitic-N (401.1 eV), and oxidic-N (403.2 eV). Among these types, pyridinic-N and pyrrolic-N species are the dominant configurations of N in CNFs-N. And these two types of N-dopants are active in increasing the Fermi level of carbon to yield improved gravimetric capacitance[25]. In addition, the N_2 adsorption-desorption curve shows the hysteresis loop of type IV (Fig. 3(d)), indicating that the CNFs-N sample exhibits a mesoporous structure with a specific surface area of 340.4 $m^2 \cdot g^{-1}$[12].

To evaluate the electrochemical performance of the CNFs-N a two-electrode cell is applied which contains two CNF-N disks of a diameter of 1cm as both the positive and negative electrodes, a PTFE

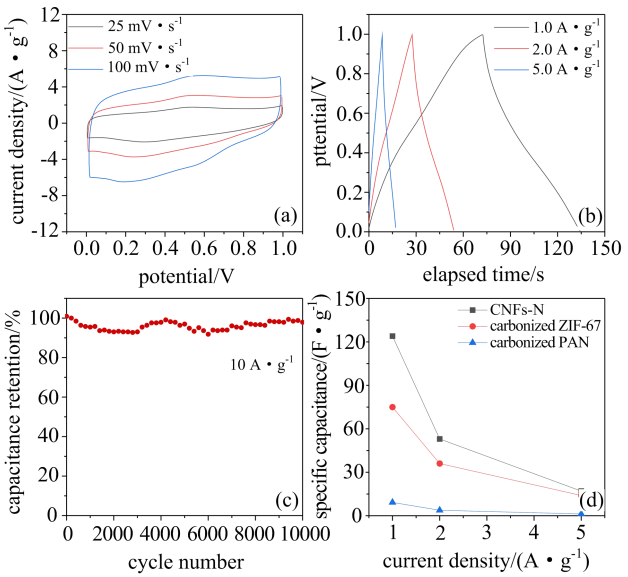

Fig. 4　(a) Cyclic voltammetry (CV) curves of the CNFs-N sample obtained at different scan rates, (b) galvanostatic charge-discharge curves at different current densities, (c) cycling performance of the CNFs-N at a current density of 10.0A • g^{-1}, (d) gravimetric capacitance of the CNFs-N and the control samples measured at different current densities

film as separator, and aqueous H_2SO_4 solution (2.0 mol • L^{-1}) as the electrolyte (See Sec. 1 for the details). The typical cyclic voltammetry (CV) curves of CNFs-N at sweep rates ranging from 25 to 100 mV • s^{-1} are presented in Fig. 4(a). The nearly rectangular shape suggests a typical capacitive behavior by the forming of an electrical double-layer at the CNF-N/electrolyte interface. The small humps can be assigned to the Faradaic reactions of Co nanoparticles decorated on the CNFs-N fibers.

Furthermore, the galvanostatic charge-discharge curves of CNFs-N (Fig. 4(b)) collected at current densities of 1.0 A • g^{-1}, 2.0 A • g^{-1}, and 5.0 A • g^{-1} present that the cell voltages are changing almost linearly with time, typical of a supercapacitor cell[26-29]. The gravimetric capacitance is 124 F • g^{-1} at current densities of 1 A • g^{-1}. In addition, the Nyquist plot of the CNFs-N shows a very low series resistance of 0.27 Ω, indicating excellent electrical conductance of the CNFs-N. Moreover, the cycling stability of

the CNFs-N is tested by galvanostatic charge-discharge at a current density of 10.0 A·g^{-1}. As shown in Fig. 4(c), the specific capacitance maintains 92% of the initial value after 10 000 cycles, indicating excellent cycling stability. On the other hand, the gravimetric capacitances of the carbonized ZIF-67 and PAN measured at 1.0 A·g^{-1} are only 75 F·g^{-1} and 10 F·g^{-1}, respectively (Fig. 4(d)), significantly lower than that of the CNFs-N, which indicates that interconnecting ZIF-67 by PAN fibers before carbonization is critical to yielding improved specific capacitance. Furthermore, we also measured the electrochemical performance of CNFs-N in 6.0 mol·L^{-1} KOH aqueous electrolyte, 1.0 mol·L^{-1} tetraethylammonium tetrafluoroborate/acetonitrile ($TEABF_4$/AN), and 1.0 mol·L^{-1} 1-butyl-3-methylimidazolium hexafluorophosphate/acetonitrile ($BMIMPF_6$/AN). The specific capacitances are 59 F·g^{-1}, 35 F·g^{-1}, and 32 F·g^{-1} at 1 A·g^{-1}, respectively, which demonstrate the possibility of CNFs-N to be applied as electrode materials for supercapacitors.

3 Conclusion

In summary, we report a CNFs-N film obtained by carbonizing a ZIF-67/PAN composite prepared by electrospun. The CNFs-N film with lateral size of tens of centimeters is assembled by microfibers which are composed of interconnected carbon spheres with N content of 6.3%. The CNFs-N exhibits a low series resistance of 0.27 Ω and specific capacitance of 124 F·g^{-1} at 1 A·g^{-1} when served as binder-free electrodes in the supercapacitor device. The specific capacitance can maintain 92% of the initial value after the CNFs-N is being cycled for 10 000 times at 10 A·g^{-1}. The good specific capacitance and cycling life and the feasibility in scaling the size of CNFs-N promise an attractive candidate for high performance supercapacitors.

References

[1] CHEN L F, LU Y, YU L, et al. Designed formation of hollow particle-based nitrogen-doped carbon nanofibers for high-performance supercapacitors[J]. Energy & Environmental Science, 2017, 10(8): 1777-1783.

[2] HUANG P, LETHIEN C, PINAUD S, et al. On-chip and freestanding elastic carbon films for micro-supercapacitors[J]. Science, 2016, 351(6274): 691-695.

[3] GEBRESILASSIE E G, ARMAND M, SCROSATI B, et al. Energy storage materials synthesized from ionic liquids[J]. Angewandte Chemie International Edition, 2014, 53(49): 13342-13359.

[4] PENG S, LI L, WU H B, et al. Controlled growth of NiMoO4 nanosheet and nanorod arrays on various conductive substrates as advanced electrodes for asymmetric supercapacitors[J]. Advanced Energy Materials, 2015, 5(2): 1401172.

[5] ZHU Y, MURALI S, STOLLER M D, et al. Carbon-based supercapacitors produced by activation of graphene[J]. Science, 2011, 332(6037): 1537-1541.

[6] SIMON P, GOGOTSI Y. Materials for electrochemical capacitors[M]//Nanoscience and Technology: A Collection of Reviews from Nature Journals. World Scientific Publishing Co Pte Ltd, 2009: 320-329.

[7] LIU J, ZHANG L, WU H B, et al. High-performance flexible asymmetric supercapacitors based on a new graphene foam/carbon nanotube hybrid film[J]. Energy & Environmental Science, 2014, 7(11): 3709-3719.

[8] PECH D, BRUNET M, DUROU H, et al. Ultrahigh-power micrometer-sized supercapacitors based on onion-like carbon[J]. Nature Nanotechnology, 2010, 5(9): 651.

[9] CHEN J, HAN Y, KONG X, et al. The origin of improved electrical double-layer capacitance by inclusion of topological defects and dopants in graphene for supercapacitors[J]. Angewandte Chemie International Edition, 2016, 55(44): 13822-13827.

[10] RAOOF J B, HOSSEINI S R, OJANI R, et al. MOF-derived Cu/nanoporous carbon composite and its application for electro-catalysis of hydrogen evolution reaction[J]. Energy, 2015, 90: 1075-1081.

[11] MAHMOOD A, ZOU R, WANG Q, et al. Nanostructured electrode materials derived from metal-organic framework xerogels for high-energy-density asymmetric supercapacitor[J]. ACS Applied Materials & Interfaces, 2016, 8(3): 2148-2157.

[12] LIU B, SHIOYAMA H, JIANG H, et al. Metal-organic framework (MOF) as a template for syntheses

of nanoporous carbons as electrode materials for supercapacitor[J]. Carbon, 2010, 48(2): 456-463.

[13] JOURNET C, MASER W K, BERNIER P, et al. Large-scale production of single-walled carbon nanotubes by the electric-arc technique[J]. Nature, 1997, 388(6644): 756.

[14] ZHANG F, MENG Y, GU D, et al. A facile aqueous route to synthesize highly ordered mesoporous polymers and carbon frameworks with Ia3d bicontinuous cubic structure[J]. Journal of the American Chemical Society, 2005, 127(39): 13508-13509.

[15] ZHENG B, LU C, GU G, et al. Efficient CVD growth of single-walled carbon nanotubes on surfaces using carbon monoxide precursor[J]. Nano Letters, 2002, 2(8): 895-898.

[16] SALUNKHE R, TANG J, KAMACHI Y, et al. Asymmetric supercapacitors using 3D nanoporous carbon and cobalt oxide electrodes synthesized from a single metal-organic framework[J]. ACS Nano, 2015, 9(6): 6288-6296.

[17] YU X Y, YU L, WU H B, et al. Formation of nickel sulfide nanoframes from metal-organic frameworks with enhanced pseudocapacitive and electrocatalytic properties[J]. Angewandte Chemie, 2015, 127(18): 5421-5425.

[18] TANG J, SALUNKHE R, LIU J, et al. Thermal conversion of core-shell metal-organic frameworks: a new method for selectively functionalized nanoporous hybrid carbon[J]. Journal of the American Chemical Society, 2015, 137(4): 1572-1580.

[19] LIU B, SHIOYAMA H, AKITA T, et al. Metal-organic framework as a template for porous carbon synthesis[J]. Journal of the American Chemical Society, 2008, 130(16): 5390-5391.

[20] DENG T, LU Y, ZHANG W, et al. Inverted design for high-performance supercapacitor via Co(OH)\—2-derived highly oriented MOF electrodes[J]. Advanced Energy Materials, 2018, 8(7): 1702294.

[21] WANG L, FENG X, REN L, et al. Flexible solid-state supercapacitor based on a metal-organic framework interwoven by electrochemically-deposited PANI[J]. Journal of the American Chemical Society, 2015, 137(15): 4920-4923.

[22] ZHANG C L, YU S H. Nanoparticles meet electrospinning: Recent advances and future prospects[J]. Chemical Society Reviews, 2014, 43(13): 4423-4448.

[23] QIAN J, SUN F, QIN L, et al. Hydrothermal synthesis of zeolitic imidazolate framework-67 nanocrystals[J]. Materials Letters, 2012, 82: 220-223.

[24] ŌYA A, ŌTANI S. Catalytic graphitization of carbons by various metals[J]. Carbon, 1979, 17(2): 131-137.

[25] CHEN J, HAN Y, KONG X, et al. The origin of improved electrical double-layer capacitance by inclusion of topological defects and dopants in graphene for supercapacitors[J]. Angewandte Chemie International Edition, 2016, 55(44): 13822-13827.

[26] ZHANG J N, LIU P, JIN C, et al. Flexible three-dimensional carbon cloth/carbon fibers/NiCo2O4 composite electrode materials for high-performance all-solid-state electrochemical capacitors[J]. Electrochimica Acta, 2017, 256: 90-99.

[27] WANG B, MACIÁ-AGULLÓ J A, PRENDIVILLE D G, et al. A hybrid redox-supercapacitor system with anionic catholyte and cationic anolyte[J]. Journal of the Electrochemical Society, 2014, 161(6): A1090-A1093.

[28] WANG B, CHEN J S, WANG Z, et al. Green synthesis of NiO nanobelts with exceptional pseudo-capacitive properties[J]. Advanced Energy Materials, 2012, 2(10): 1188-1192.

[29] LI Y, WANG G, WEI T, et al. Nitrogen and sulfur co-doped porous carbon nanosheets derived from willow catkin for supercapacitors[J]. Nano Energy, 2016, 19: 165-175.